Proceedings of the 7th GACM Colloquium on Computational Mechanics for Young Scientists from Academia and Industry October 11-13, 2017 in Stuttgart, Germany

Modelling of the Mars® 300 armour steel under impact loadings

Fras Teresa[1]*, Faderl Norbert[1] and Lach Erhardt[1]

Micro Abstract
Material and protective properties of the Mars® 300 steel are analyzed to understand the steel behavior under impact loadings. To validate the flow and fracture model (the Hosford-Coulomb model), a numerical simulation of the impact configuration is performed in which the striker and target are made of the Mars® 300 steel. As targets, plates perforated by an array of holes applied as passive add-on armors in combat vehicles - are considered.

[1]PCE - Explosive and Ballistic Protection, French-German Research Institute of Saint-Louis (ISL), Saint-Louis, France

***Corresponding author**: teresa.frs@gmail.com

Introduction

Mars® 300 belongs to a group of steels dedicated to ballistic protection as its properties, especially high hardness and strength, provide high level of ballistic performances. The steel may be used as a perforated passive add-on armor, a relatively thin steel plate with an array of punched holes, which is fixed in front of the main armor. A regular holes pattern in steel sheets increases the probability of asymmetrical contact between the plate and small-caliber projectiles, due to which projectiles may be destabilized or fragmented before they reach the main-armor. It is observed that depending on the hit-position, the projectile core may break into pieces or it may be partially eroded and rotated, [1–3].

To determine the strain to fracture and to obtain an accurate description of the local strain fields at very large deformations, the hybrid experimental-numerical approach is applied. The results are employed to calibrate a plasticity model with a Johnson-Cook type of rate and temperature-dependency and a combined Swift-Voce strain hardening law used in conjunction with a non-associated anisotropic flow rule, [4, 5].

1 Impact experiments

The impact tests are carried out to investigate impact properties of the Mars 300 steel. The steel is available as homogenous plates but also as perforated plates of different thicknesses and hole size. The thickness and size of the holes have to be specified against a particular threat. The chosen add-on plates have geometrical characteristics due to which they may be applied against impacts of hard-core 7.62 mm P80 0.30 AP x 51 (.308 Win) projectiles. As small-calibre projectiles consist of several components made from different materials, i.e. very hard steel, lead and brass; adequate modeling of such multi-body interactions requires a thorough understanding of the material properties for each of them, as well as their geometrical and frictional characteristics. Instead of such a multi-body threat, single-material threats were impacted into plates. Cylindrical impactors with a length of 30 mm and a diameter of 5 mm, resulting in a mass of 4.7g, are cut by wire EDM from homogenous Mars 300 plates with an initial thickness of 6 mm, Figure 1. In the manufacturing process, circular holes are punched in the base material before the heat treatment. Due to this process, the holes have a slight conical shape, with an average diameter on the front of 5mm and an average diameter of 5.35 mm on the back side.

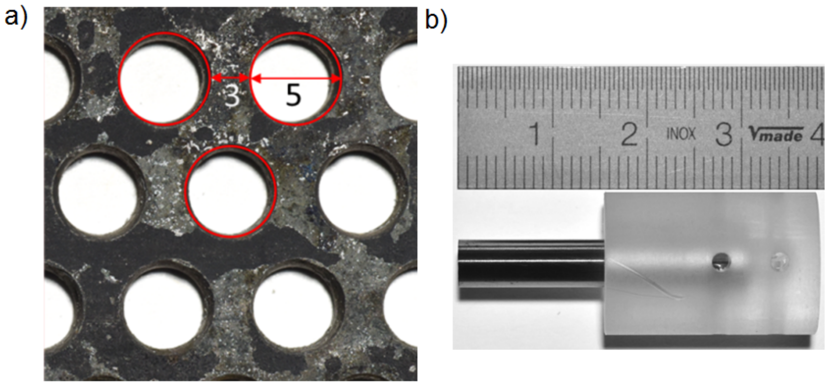

Figure 1. Components for the impact experiments: a) close-up of the hole pattern in the perforated Mars® 300 plate (mm) (front face) and b) Mars® 300 impactor in a sabot.

All impact experiments are conducted at room temperature using a high-pressure single-stage gas gun, Figure 2. For the given mass of a projectile and a polyethylene sabot (4.1 g), the peak performance of the launching system results in an impact velocity of approximately 450 m/s measured by a double-laser light barrier located near the exit of the gun muzzle. Each impact is monitored by three high speed cameras which allow for observations from different angles.

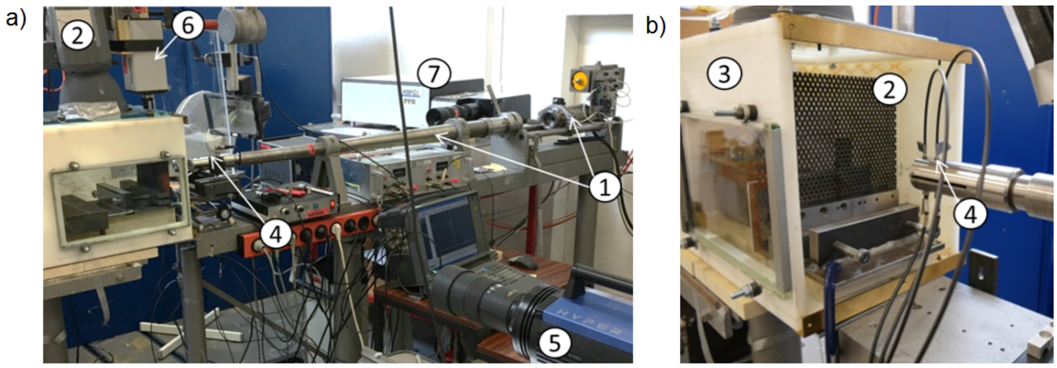

Figure 2. Experimental set-up for the impact tests: 1-single-stage gas gun, 2-specimen mounted in 3-catch box, 4-gun barrel with double-laser light barrier, 5-Shimadzu HPV1 high-speed camera for the side view, 6-SensiCam short-time camera for the top view and 7-HSFC Pro camera registering impact positions.

A total of 15 impact experiments in Mars 300 plates of the size 200x200 mm and a thickness of 4 mm at impact speeds ranging from 400 m/s to 450 m/s are carried out. The aim of the experiment is to investigate the dependence between plate damage pattern and the location of the impactor upon an impact. Three representative impact cases are identified and analyzed with regard to the impact position and the damage pattern, Figure 3.

2 Finite element analysis of impact tests

All simulations are carried out using the dynamic explicit solver of Ls-Dyna R9.0.1. All components are meshed with reduced integration 8-node constant-stress solid elements with stiffness-based hourglass control. The impact zone together with the cylindrical impactor are discretized with a fine mesh of element edge length.

This refined zone stretches over a square area of diameter 15 mm for the homogenous plate; for the perforated plate, it covers a rectangular area of 624 mm^2. The shape of the punched holes is accurately modelled by changing the diameter from 5 mm on the front surface to 5.3 mm on

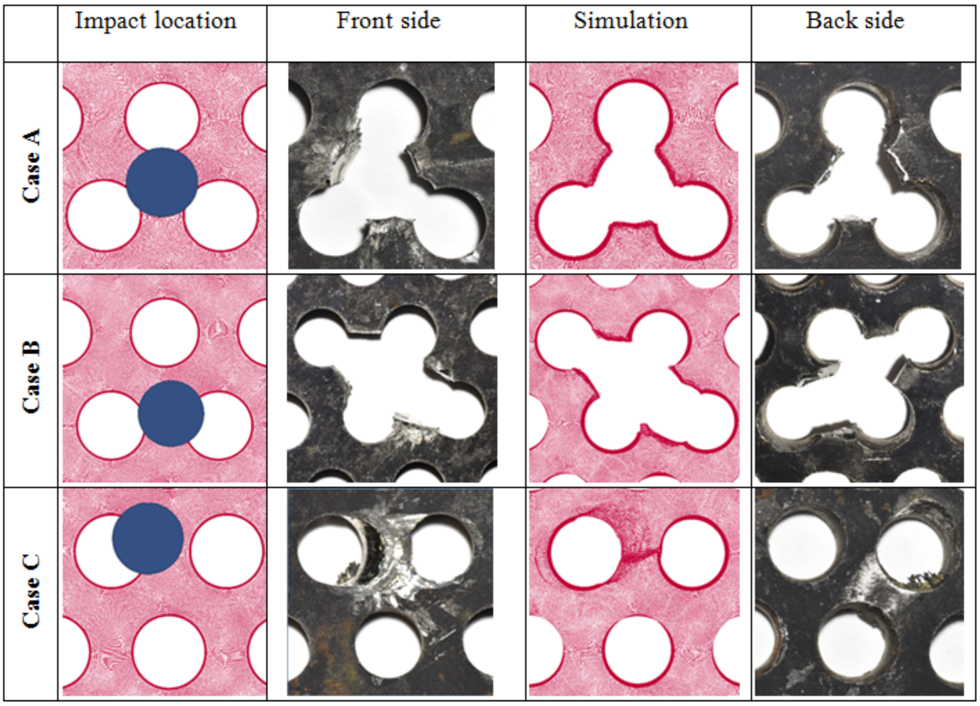

Figure 3. Impact positions and damage patterns of the three representative impact cases in the perforated plates - experimental and numerical comparison.

the back face. The total number of elements is about 900000 for the homogenous plate while 2000000 are used for the perforated plate and 260000 for the impactor. All boundary conditions are imposed as observed in the experiment - plates are clamped on their edges and the measured impact velocity is imposed on the cylinder as an initial condition. The plasticity and fracture model are applied with a user material subroutine (since R9.0.1 both models could also be used from $*MAT\_260B$ in the commercial package). A frictionless contact is chosen between the plate and the impactor with the contact option *ERODING_SURFACE_TO_SURFACE, which allows for element erosion.

When a projectile hits centrally between three holes, it solely affects the part of the plate directly below the projectile. The material is pushed by the striker with a high strain rate while the surrounding material remains motionless. The shape of the forming plug can already be recognized at 8 μs and a crack initiates on the back side of the plate at 9 μs. At 12 μs, when the depth of striker penetration has not even reached 1 mm of the plate thickness, the fully formed plug is separated from the plate. This moment is also indicated by a distinct reduction of the striker's impact velocity. After the plate perforation, the velocity of the striker remains nearly constant. With the impact position of the cylinder being fully symmetrical to 3 holes and perfectly perpendicular to the plate, its trajectory after the plate perforation remains unaltered. These perfect geometrical features and boundary conditions could also explain the slight overestimation of approximately 15% in the residual velocity as compared to the experiment.

Different from the previous case, the impact position of the cylinder is not symmetrical in relation to the surrounding holes. Shearing is induced between the plate part compressed dynamically by the moving striker and a part, which is stable. As the contact between the target and the impactor is not symmetrical, the shear bands initiate at different time steps. The formed debris has a free end, while the opposite side is still attached to the plate. As the cylinder continues to push this free end, the debris behaves similarly to a bent cantilever beam. This complex state leads to the formation of two additional shear bands in the narrowest part of the plate. The numerically obtained residual velocity of the striker is in good agreement with the value measured experimentally. Two sudden drops of the striker velocity occur when the first and then the second ligament of the debris fail and disconnect from the plate.

When the projectile hits exactly in a hole or partly in a hole and in the material, then the impactor slips through the hole causing some plastic deformation, but almost no damage to the plate. Traces of the contact between the striker and the plate are represented in the simulation. Since its deviation depends on the contact with the inner surfaces of the hole, the trajectory of the striker after passing through a hole is difficult to predict.

Conclusions

The complexity of the conditions leading to failure of the perforated, high-strength steel plates is shown. The small extension of the damage zones in the target plate proves the applicability of this armor solution against multiple small-caliber impacts. When a plug is ejected from the plate, shearing is the globally dominant mechanism between the moving projectile and the motionless plate. The trajectories of the cylinders after plate perforation, as well as the values of the residual velocity are in agreement with the experimentally obtained ones. It is found that the chosen plasticity and fracture models can describe impact scenarios and the fracture patterns in both the homogenous as well as the perforated plates with good accuracy.

References

[1] T. Fras, A. Murzyn, and Pawlowski. Defeat mechanism provided by slottted add-on bainitic plates against small-calibre 7.62mm x 51 ap projectiles. *Int J Impact Eng*, Vol. 103:p. 241–53, 2017.

[2] T. Fras and C. Roth. Fracture of high strength armour steel under impact loading. *Int J Impact Eng*, 2017.

[3] P. Pawlowski and T. Fras. Numerical and experimental investigation of asymmetrical contact between a steel plate and armour-piercing projectiles. In *11th European Ls-Dyna Conference 2017, Salzburg, Austria*, 2017.

[4] C. Roth and D. Mohr. Effect of strain rate on ductile fracture initiation in advanced high strength steel sheets: experiments and modeling. *Int J Plasticity*, Vol. 56:p. 19–44, 2014.

[5] C. Roth and D. Mohr. Ductile fracture experiments with locally proportional loading histories. *Int J Plasticity*, Vol. 79:p. 328–54, 2016.